Physical properties of a regular rotating black hole: Thermodynamics, stability, and quasinormal modes

S. H. Hendi,[1,2,3,†] S. N. Sajadi,[1,2,*] and M. Khademi[4,‡]

[1]*Department of Physics, School of Science, Shiraz University, Shiraz 71454, Iran*
[2]*Biruni Observatory, School of Science, Shiraz University, Shiraz 71454, Iran*
[3]*Canadian Quantum Research Center, 204-3002 32 Ave Vernon, BC V1T 2L7 Canada*
[4]*Department of Physics, Shahid Beheshti University, G. C., Evin, Tehran 19839, Iran*

(Received 20 June 2020; accepted 11 February 2021; published 10 March 2021)

Respecting the angular momentum conservation of torque-free systems, it is natural to consider rotating solutions of massive objects. Besides that, motivated by the realistic astrophysical black holes that rotate, we consider a nonlinearly charged regular rotating black hole. We investigate the geometrical properties of the metric by studying the boundary of ergosphere. We also analyze thermodynamic properties of the solution in anti–de Sitter spacetime and examine thermal stability and the existence of phase transition. In addition, we perturb the black hole by using of a real massless scalar field as a probe to investigate its dynamic stability. We also obtain an analytic expression for the real and imaginary parts of the quasinormal frequencies.

DOI: 10.1103/PhysRevD.103.064016

I. INTRODUCTION

One of the main open questions in theoretical physics is the existence of singularity in different theories. From the gravitational point of view, there might be something mysterious about the spacetime singularity. Thus, investigation of such a pathology is a hot topic, either in physical and mathematical communities or in philosophical circles.

The Einstein general relativity not only admits different solutions including singularity, but expresses that such a singularity may be unavoidable a real-world scenario. For this reason, one has to perceive the nature of singularity to understand the nature of singular spacetimes. Nonetheless, since the general relativity could not describe the nature and physical properties of the spacetime singularity, one may look for alternative viewpoint. The possibility of constructing a nonsingular (regular) spacetime might be potentially important implication for avoiding the breakdown of physical laws near the singularity, a region with extreme curvature and vanishing volume. In addition, there is as yet no consistent theory of quantum gravity and some scientists believe that the singularity would not occur in such a theory. Fortunately, the Einstein general relativity allows some regular solutions without curvature singularity which contain at most coordinate singularity [1]. It is worth mentioning that such regular black holes are not vacuum solutions of the Einstein field equations. These regular solutions often include a special class of nonlinear electrodynamics violating energy conditions in the vicinity of the black hole [2–8]. Till date there has been a lot of significant work in regular solutions of gravitating systems [9–21].

On the other hand, according to the published results of the gravitational wave observatories by the collaborations LIGO and VIRGO [22–24] and shadow of black hole by Event Horizon Telescope [25–28], one finds that the astrophysical black holes are not static and spherically symmetric, but asymmetric due to they have rotation. In other words, one of the most realistic features of relativistic black holes is that they have angular momentum in a stationary manner. Hence, in order to have a pragmatic black hole solution, one has to consider rotating spacetime. However, introducing a new rotating black hole solution, directly, is a nontrivial task as it turns out to be a rather long process to obtain the Kerr solution. However, one may use the Newman-Janis algorithm to convert static solutions to rotating ones [29–37]. A special solution of the Kerr black hole in the presence of electromagnetic field is obtained in [38]. Phase transition of the Kerr-Newman-AdS (anti–de Sitter) black hole with a model of dark energy is discussed in [39] and its extension to nonlinear magnetic charge in [40]. The astrophysical aspects of rotating black holes, such as shadow images and the geodetic precession frequency, have already been studied in [41,42]. Besides that, other physical properties of rotation black holes, in particular thermodynamic behavior and photon sphere are of interest.

Taking into account the quantum effects near a black hole, one has to regard it as a thermodynamical entity with a temperature and an entropy. Such a statement help us to

*Corresponding author.
naseh.sajadi@gmail.com
†hendi@shirazu.ac.ir
‡Maryam.Khademi@obspm.fr

understand a deep connection among three interesting theories: general relativity, quantum field theory and thermodynamics. In other words, the black hole thermodynamics can be used as a bridge to connect two apparently independent theories: general relativity and quantum field theory. Black hole thermodynamics began, seriously, with the pioneering works of Hawking and Beckenstein, and has recently become very fascinating in the extended phase space by considering the cosmological constant as a thermodynamic quantity. Taking a dynamical cosmological constant $\Lambda = -8\pi P$ into account, the consistent first law of black hole thermodynamics and the associated Smarr relation are modified by including a PV term. Comparing such a modified first law of black hole thermodynamics with that of everyday system, we find that, in this representation, the mass of the black hole M is considered as the enthalpy of the system instead of the internal energy [43–61]. Exploring the phase transition and critical behavior of the black hole solutions in the extended phase space is another interesting issue which is reported for different gravitating systems [54–58]. Thermal stability of a black hole plays an important role in exploring its behavior near the equilibrium. It is notable that a thermally stable black hole has a non-negative heat capacity.

In addition to thermal stability criteria, one has to examine dynamical stability of black holes under perturbations of the geometry and matter fields. The robustness check of black holes against small perturbations is sufficiently strong to veto some mathematical black holes. Regarding a perturbative black hole, one may observe some oscillated behavior, named as quasinormal modes (QNMs) which are related to some quasinormal frequencies (QNFs). It is shown that QNMs are the intrinsic imprints of the black hole response to external perturbations which means that such QNMs are independent of initial perturbations. The authors of Refs. [62,63] show that the asymptotic behavior of QNMs is related to the quantum nature of gravitation. It is also reported that for AdS black holes, the imaginary parts of QNFs are corresponding to the perturbations damping of a thermal state in the conformal field theory [64,65]. So, the investigation of QNMs help us to find the features of compact objects, the evolution of fields and also the properties of spacetime [66–68].

There are several approaches to the study black hole's QNMs. Ferrari and Mashhoon [69,70], working on the potential barrier in the effective one-dimensional Schrödinger equation and obtain simple exact solutions. Such a barrier is related to the photon sphere of the black hole [71]. We should note that QNMs of regular black holes have been studied before [72–74]. The behavior of QNMs at the thermodynamics phase transitions has been studied in [75,76]. Moreover, the relation between the QNFs and the thermodynamical quantities at eikonal limit for static solution [77] and for rotating one [78] has been studied. Cardoso *et al.* [79] showed that the real part of the QNMs is related to the angular velocity of the last circular null geodesic while Stefanov *et al.* [80] found a connection between black hole's QNMs in the eikonal limit and lensing in the strong deflection limit. Furthermore, in Ref. [81] the connection between the QNMs and the shadow radius for static black hole and recently for rotating one [82] has been obtained.

The paper is organized as follows. In Sec. II, we study the geometric properties of an interesting class of regular rotating black hole. We study the thermodynamics of rotating AdS black hole and look for possible phase transition in Sec. III. Section IV is devoted to study the QNMs and their connection to the properties of photon sphere in the eikonal limit. The paper ends with our concluding remarks in Sec. V.

II. REGULAR ROTATING BLACK HOLE

The four-dimensional action governing nonlinearly charged black holes in the presence of a negative cosmological constant is given by

$$\mathcal{A} = \frac{1}{16\pi}\int d^4x\sqrt{-g}\left[\mathcal{R} + \frac{6}{l^2} - \mathcal{L}(\mathcal{F})\right], \tag{2.1}$$

in which g is the determinant of the metric tensor, $l = \sqrt{-3/\Lambda}$ denotes the AdS length related to the negative cosmological constant, $\mathcal{R}$ is the Ricci scalar and $\mathcal{L}(\mathcal{F})$ is an arbitrary function of the Maxwell invariant $\mathcal{F} = \mathcal{F}_{\mu\nu}\mathcal{F}^{\mu\nu}$. Applying the variational principle to the action (2.1), one can show that the field equations are given by

$$G_{\mu\nu} - \frac{3}{l^2}g_{\mu\nu} = 2\mathcal{L}_{\mathcal{F}}\mathcal{F}_{\mu\lambda}\mathcal{F}^{\lambda}_{\nu} - \frac{1}{2}g_{\mu\nu}\mathcal{L}(\mathcal{F}), \tag{2.2}$$

$$\nabla_{\mu}(\mathcal{L}_{\mathcal{F}}\mathcal{F}^{\mu\nu}) = 0, \tag{2.3}$$

where in the above equations $G_{\mu\nu}$ is the Einstein tensor and $\mathcal{L}_{\mathcal{F}} = d\mathcal{L}/d\mathcal{F}$.

The metric of rotating charged regular black hole in the Boyer-Lindquist coordinates is obtained as [29,30]

$$dS^2 = -\frac{\Delta_r}{\Sigma}\left(dt - \frac{a\sin^2(\theta)}{\Xi}d\phi\right)^2 + \frac{\Sigma}{\Delta_r}dr^2 + \frac{\Sigma}{\Delta_\theta}d\theta^2 + \frac{\Delta_\theta\sin^2(\theta)}{\Sigma}\left(adt - \frac{r^2+a^2}{\Xi}d\phi\right)^2, \tag{2.4}$$

where

$$\Delta_r = (r^2+a^2)\left(1+\frac{r^2}{l^2}\right) - 2f,$$

$$\Sigma = r^2 + a^2\cos^2\theta,$$

$$\Xi = 1 - \frac{a^2}{l^2},$$

$$\Delta_\theta = 1 - \frac{a^2}{l^2}\cos^2\theta,$$

and the functional form of $f(r)$ depends on the choice of the electromagnetic Lagrangian $\mathcal{L}(\mathcal{F})$. Our approximate functional form of $f(r)$ is introduced in [6,7] as

$$f(r) = Mr\exp\left(-\frac{q^2}{2Mr}\right). \tag{2.5}$$

Although for the sake of simplicity we have considered the above exponential form of $f(r)$, there are additional reasons supporting such a functional form. The asymptotic behavior of the metric (2.4) with (2.5) is the Kerr-Newman-AdS black hole. Besides, this rotating regular metrics is the same as the Kerr black hole in such a way that the mass m of the Kerr black hole is replaced by $m(r)$. Moreover, the exponential convergence factor is used in the formulation of the quantum gravity that is finite to all order in the Planck length [83]. The inclusion of such quantum gravity effects makes other flat space quantum field theories similarly finite. Also a finite quantum gravity theory can be used to resolve the cosmological constant problem [7,84].

The radius of the horizon r_+ can be obtained from the following equation

$$\Delta_r|_{r=r_+} = (r_+^2 + a^2)\left(1 + \frac{r_+^2}{l^2}\right) - 2Mr_+\exp\left(\frac{-q^2}{2Mr_+}\right) = 0.$$

The existence/nonexistence of real positive root of the above equation indicates two scenarios: a regular black hole or no-horizon solution. The regular black hole and no-horizon cases may be separated by introducing the extremal horizon of the black hole solution. The extremality condition is defined by the following relation

$$\Delta_r|_{r=r_+} = \Delta_r'|_{r=r_+} = 0.$$

Regarding $\Delta_r(r = r_+) = 0$, one can obtain

$$M = \frac{q^2}{2r_+\mathcal{W}\left(\frac{l^2q^2}{(l^2+r_+^2)(a^2+r_+^2)}\right)}, \tag{2.6}$$

where $\mathcal{W}$ is the "*Lambert W*" function satisfying $\mathcal{W}(x)\exp(\mathcal{W}(x)) = x$ (see [85] for more details). It is notable that M has a minimum which is corresponding to the extremal configuration for the black hole. So, by taking the derivative of mass with respect to the horizon radius, one can obtain the extremal charge which its maximum value is

$$q_{\max}^2 = \left(r_+^2 - a^2 + \frac{r_+^2(3r_+^2 + a^2)}{l^2}\right) \times \exp\left(\frac{3r_+^4 + r_+^2(a^2 + l^2) - a^2l^2}{r_+^4 + r_+^2(l^2 + a^2) + a^2l^2}\right). \tag{2.7}$$

For the case of $M = l = 1$, one can obtain the following relation between the extremal value of quantities

$$q_{\text{ext}} = \sqrt{2r_+\left(1 + \frac{1 - r_+^2}{1 + r_+^2}\mathcal{W}\right)}, \tag{2.8}$$

and

$$a_{\text{ext}} = \left(-1 - \frac{2}{\mathcal{W}}\right)^{1/2} r_+, \tag{2.9}$$

where $W = W(-r_+(r_+^2 + 1)\exp(\frac{r_+^2-1}{r_+^2+1}))$.

The conditions of having the regular black hole or the no-horizon solution in terms of the free parameters are observed in Fig. 1. In order to have regular black holes, there are upper limits (critical values) on the electric charge and rotation parameter of the metric. At the critical values (the border of the shaded and white regions) there is a minimum horizon which corresponds to the extremal black hole (a-r plot). The solution has no-horizon in the white region of the a-q plot. In the case of the rotating regular black hole (shaded region of a-q plot), by increasing the rotation parameter a the critical value of the electric charge decreases.

Static observers cannot exist everywhere in the spacetime, because the four velocity of static observer finally becomes null. When this occurs the observer cannot remain static and rotate with the black hole. Therefore, the stationary limit surface is described by $g_{tt} = 0$. Similar to the case of event horizon, one can obtain the conditions for the critical parameter of black hole so that the solutions of $(g_{tt} = 0)$ merge to one. The conditions are

$$g_{tt} = \partial_r g_{tt} = 0. \tag{2.10}$$

Solving the mentioned conditions, simultaneously, for obtaining q and r in the case of $M = l = 1$, $\theta = \pi/2$ and plotting them, one can find Fig. 2 and obtain following equations

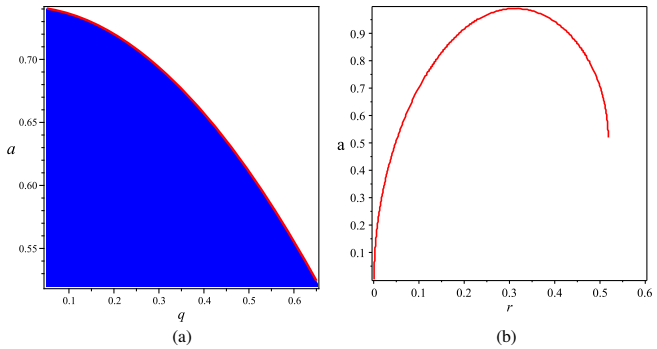

FIG. 1. The behavior of the critical value of the magnetic charge q and radius of the event horizon r in terms of the rotation parameter a for $M = 1$, $l = 1$. Notice that the a-r plots are at the critical values of q.

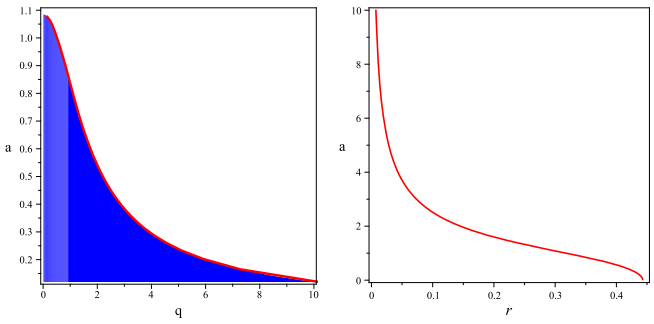

FIG. 2. The behavior of the critical value of the magnetic charge q and radius of the stationary limit surface r in terms of the rotation parameter a for $M = 1$, $l = 1$, $\theta = \pi/2$. Notice that the a-r plots are at the critical values of q.

$$q = \sqrt{2r[1 - \mathcal{W}(-r^3 e)]},$$
$$a = \sqrt{-\left(1 + r^2 + \frac{2r^2}{\mathcal{W}(-r^3 e)}\right)}, \tag{2.11}$$

where $e = \exp(1)$. In the a-q plot, shaded and white plots correspond to the regular black hole with stationary limit surface and without stationary limit surface, respectively. The a-r plot represents the dependence of the radius of the stationary limit surface on a. The stationary limit surface does not coincide with the event horizon and is located outside the horizon. The region between the horizon and the stationary limit surface is called the ergoregion which is shown in the Fig. 3. In Fig. 3, size and shape of ergoregion in the z-x plane, where $z = r\cos\theta$ and $x = r\sin\theta$, have been depicted. By increasing q and a, one can observe the change in the shape and size of the ergoregion.

We now consider a possible nonlinear source for the metric (2.4). The magnetic part of the gauge field (A^m_μ) of charged rotating regular black hole is given by

$$A^m_\mu = -\frac{qa\cos\theta}{\Sigma}\delta^t_\mu + \frac{q(r^2 + a^2)\cos\theta}{\Xi\Sigma}\delta^\phi_\mu, \tag{2.12}$$

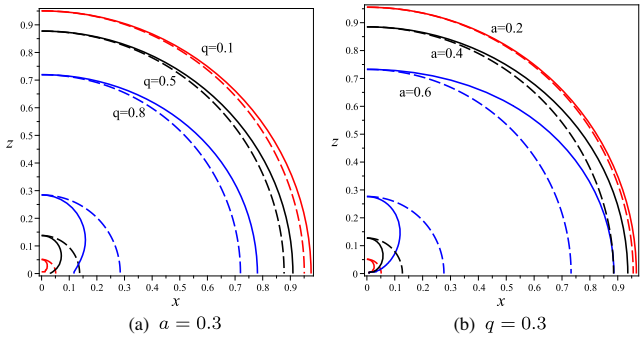

FIG. 3. Horizons (dashed line) and stationary limit surfaces (solid line) for different values of a and q are depicted in the figures.

in which by calculating the electromagnetic field tensor, one obtains

$$\mathcal{F} = F_{\mu\nu}F^{\mu\nu} = \frac{2q^2(r^4 - 6r^2a^2\cos^2\theta + a^4\cos^4\theta)}{\Sigma^4}. \tag{2.13}$$

By solving the Einstein tensor for $\mathcal{L}$ and $\mathcal{L}_\mathcal{F}$ as independent quantities, one can find

$$\mathcal{L} = -\frac{6}{l^2} + \frac{8r^2a^2\cos^2\theta\Sigma f''}{\Sigma^4} + \frac{2(rf' - f)\mathcal{F}}{q^2}, \tag{2.14}$$

$$\mathcal{L}_\mathcal{F} = \frac{-\Sigma f'' + 4(rf' - f)}{2q^2}. \tag{2.15}$$

The above definitions for $\mathcal{L}$ and $\mathcal{L}_\mathcal{F}$ satisfy all five different Einstein field equations. In the case of $a = 0$, one can recover the expressions presented in [86]. Here, we have to check the consistency between Eqs. (2.14) and (2.15). To do so, we should check whether the total derivative of $\mathcal{L}$ [in Eq. (2.14)] with respect to $\mathcal{F}$ is equal to $\mathcal{L}_\mathcal{F}$ [presented in Eq. (2.15)]. So, the difference between the total derivative of Eq. (2.14) with respect to $\mathcal{F}$ and Eq. (2.15) in the case of $\theta = \theta_0 =$ constant is given as

$$\Delta\mathcal{L}_\mathcal{F} = \mathcal{L}_\mathcal{F} - \frac{\partial\mathcal{L}}{\partial\mathcal{F}} = \mathcal{L}_\mathcal{F} - \frac{\partial\mathcal{L}}{\partial r}\frac{\partial r}{\partial\mathcal{F}} \neq 0, \tag{2.16}$$

where its asymptotic limit ($r \gg 1$) is

$$\Delta\mathcal{L}_\mathcal{F} \approx \frac{-5q^2a^2\cos^2\theta_0}{4Mr^3} + \frac{3q^4a^2\cos^2\theta_0}{4M^2r^4} + \mathcal{O}\left(\frac{1}{r^5}\right). \tag{2.17}$$

In Fig. 4, we have shown $\Delta\mathcal{L}_\mathcal{F}$ in terms of r at the equatorial plane of the regular rotating black holes for

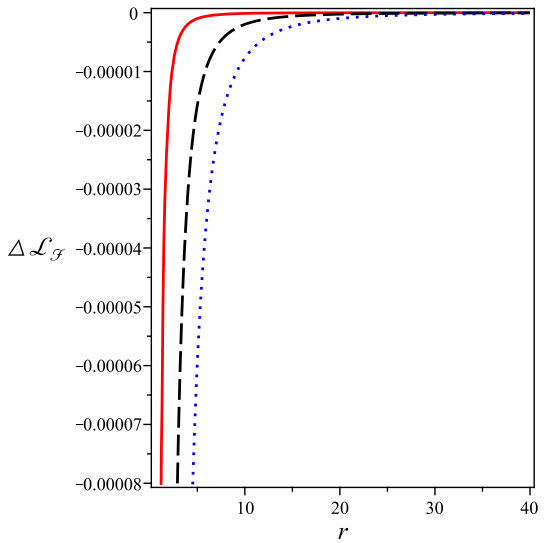

FIG. 4. The behavior of $\Delta\mathcal{L}_\mathcal{F}$ in terms of r at $\theta = 0$ for $M = 1$, $a = 0.1$, $q = 0.1$, 0.4, 0.8 (red to blue).

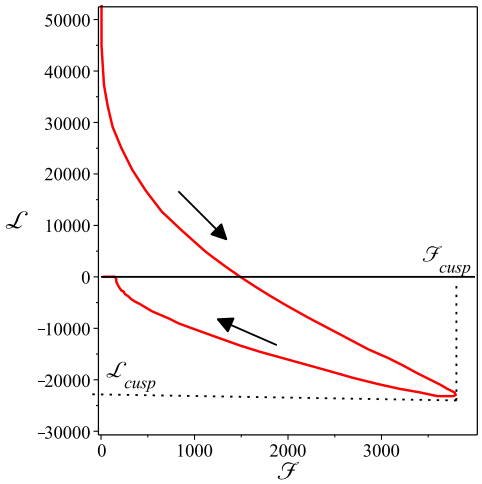

FIG. 5. The behavior of $\mathcal{L}(\mathcal{F})$ in terms of $\mathcal{F}$ at $\theta = \pi/2$ for $M = 1$, $a = 0.5$, $q = 0.5$.

different values of parameters. According to the Fig. 4, one finds that the inconsistency between $\mathcal{L}_{\mathcal{F}}$ and $\partial\mathcal{L}/\partial\mathcal{F}$ is smaller than 10^{-4}. As a result, we find that the metric (2.4) is a charged rotating solution for the Einstein equation.

According to Fig. 5, the function $\mathcal{L}(\mathcal{F})$ has two branches. Indeed, the Lagrangian $\mathcal{L}(\mathcal{F})$, first decreases smoothly along the first branch (upper) from its maximum value to $\mathcal{L}_{cusp}$ as $\mathcal{F}$ increases from $\mathcal{F} = 0$ at $r = 0$ to $\mathcal{F}_{\min} = \mathcal{F}_{cusp}$. Then, the Lagrangian increases along the second branch (lower) from its minimal value $\mathcal{L}_{cusp} < 0$ to its Maxwell limit $\mathcal{L} \to \mathcal{F} \to 0$ as $\mathcal{F}$ decreases from $\mathcal{F}_{cusp}$ to $\mathcal{F} \to 0$ ($r \to \infty$).

III. THERMODYNAMICS

In this section, we explore the thermodynamics of the regular rotating-AdS black hole solution (2.4). In order to investigate the thermodynamic properties of the black hole in extended phase space, we need to obtain some relevant thermodynamic quantities. In the extended phase space, we treat the cosmological constant as a thermodynamic pressure and its conjugate quantity as a thermodynamic volume via [51,52,59]

$$P = \frac{3}{8\pi l^2}, \qquad V = \frac{r_+ A}{3} + \frac{4\pi J^2}{3\mathcal{M}}, \tag{3.1}$$

where A is the horizon area of black hole which is calculated as

$$A = \int_0^{2\pi}\int_0^{\pi} \sqrt{g_{\theta\theta}g_{\phi\phi}}\, d\theta d\phi \Big|_{r_+} = \frac{4\pi(r_+^2 + a^2)}{\Xi}, \tag{3.2}$$

and $\mathcal{M}$ and J are, respectively, the mass and the angular momentum of the black hole which can be obtain by using of Altas-Tekin method [87]. Using the Killing vectors $k^\mu = \delta^\mu_t/\Xi$ and $k^\mu = \delta^\mu_\phi$ associated with the time translation and rotational invariance, one gets [88]

$$J = \frac{Ma}{\Xi^2}, \qquad \mathcal{M} = \frac{M}{\Xi^2}. \tag{3.3}$$

The Hawking temperature for nonextremal case can be obtained by using the surface gravity interpretation

$$\begin{aligned} T &= \frac{\kappa}{2\pi} = \frac{1}{4\pi(a^2 + r_+^2)} \frac{d\Delta_r}{dr}\Big|_{r_+} \\ &= -\frac{(2Mr_+ + q^2)e^{-\left(\frac{q^2}{2Mr_+}\right)}}{4\pi(r_+^2 + a^2)r_+} + \frac{r_+(r_+^2 + 2r_+^2 + a^2)}{2\pi l^2(r_+^2 + a^2)}, \end{aligned} \tag{3.4}$$

where κ is the surface gravity. In the case of small q and a we have

$$\begin{aligned} T = {} & \frac{1}{4\pi r_+}\left(1 + \frac{3r_+^2}{l^2} - \frac{q^2}{r_+^2}\right) \\ & - \frac{1}{4\pi r_+^3}\left[2 + \frac{2r_+^2}{l^2} - \frac{q^2}{r_+^2}\right]a^2 + \mathcal{O}(q^3, a^4). \end{aligned} \tag{3.5}$$

As we know, the Killing vector $k^\mu = \delta^\mu_t + \Omega\delta^\mu_\phi$ at the event horizon of the rotating black hole is a null vector, and therefore, we can use

$$k_\mu k^\mu = g_{tt} + 2\Omega g_{t\phi} + \Omega^2 g_{\phi\phi} = 0 \tag{3.6}$$

to obtain the angular velocity, Ω, by inserting g_{tt}, $g_{t\phi}$ and $g_{\phi\phi}$ from the metric (2.4)

$$\begin{aligned} \Omega = {} & \frac{a\Xi((r_+^2 + a^2)\Delta_\theta - \Delta_r)}{\Delta_\theta(r_+^2 + a^2)^2 - \Delta_r a^2 \sin^2(\theta)} \\ & \pm \frac{\Xi\Sigma\sqrt{\Delta_r\Delta_\theta}}{(\Delta_r a^2 \sin^2(\theta) - \Delta_\theta(r_+^2 + a^2)^2)\sin(\theta)}, \end{aligned} \tag{3.7}$$

on the horizon $\Delta_r(r_+) = 0$, so we obtain following expression for angular velocity

$$\Omega_+ = \frac{a\Xi}{r_+^2 + a^2}. \tag{3.8}$$

However, we should note that the thermodynamical angular velocity is the differences between the angular velocity measured by the observer at the infinity and the angular velocity at the horizon, yielding

$$\Omega = \Omega_+ - \Omega_\infty = \Omega_+ + \frac{a^2}{l^2} = \frac{a}{r_+^2 + a^2}\left(1 + \frac{r_+^2}{l^2}\right). \tag{3.9}$$

The electric part of vector potential is given as

$$A^e_\mu = -\frac{qr}{\Sigma}\delta^t_\mu + \frac{qar\sin^2(\theta)}{\Sigma\Xi}\delta^\phi_\mu, \tag{3.10}$$

so the electrostatic potential of the event horizon with respect to spatial infinity as an electrostatic potential reference is obtained as

$$\Phi = A^e_\mu k^\mu|_\infty - A^e_\mu k^\mu|_{r_+} = \frac{qr_+}{r_+^2 + a^2}, \tag{3.11}$$

where $k^\mu = \delta^\mu_t + \Omega_+\delta^\mu_\phi$ is the null generator of the horizon. By computing the flux of electromagnetic field tensor by using of the standard Gauss's law, one can obtain the electric charge as follow

$$Q = \frac{1}{4\pi}\int \star F = \frac{q}{\Xi}, \tag{3.12}$$

where $\star F$ is the dual of the Faraday 2-form. For a black hole embedded in AdS spacetime, employing the relation between the cosmological constant and thermodynamic pressure, would result in the interpretation of the black hole mass as the enthalpy. Using the expressions (3.3), (3.12) and (3.2) for mass, angular momentum, electric charge and entropy, and the fact that $\Delta_r(r_+) = 0$, one obtains the enthalpy in terms of thermodynamic quantities as

$$H = \mathcal{M} = \left(\frac{8\pi PJ^2}{3} + \frac{\pi J^2}{S} + \frac{\pi Q^4}{S\Upsilon^2}\right)^{\frac{1}{2}},$$
$$\Upsilon = \mathcal{W}\left(\frac{3\pi Q^2}{8PS(S+\frac{3}{8P})}\right) \tag{3.13}$$

by using (3.13), one can determine the temperature, electrostatic potential, volume and angular momentum, respectively, as

$$T = \left(\frac{\partial H}{\partial S}\right)_{Q,P,J} = -\frac{\pi J^2}{2\mathcal{M}S^2} - \frac{\pi Q^4[\Upsilon(PS+3/8)-(3SP+3/8)]}{\mathcal{M}S^2\Upsilon^2(1+\Upsilon)(3+8PS)}, \tag{3.14}$$

$$\Phi = \left(\frac{\partial H}{\partial Q}\right)_{S,P,J} = \frac{\pi Q^3}{2\mathcal{M}S\Upsilon(1+\Upsilon)}, \tag{3.15}$$

$$V = \left(\frac{\partial H}{\partial P}\right)_{Q,S,J} = \frac{4\pi J^2}{3\mathcal{M}} + \frac{2\pi Q^4}{\mathcal{M}(3+8PS)\Upsilon^2(1+\Upsilon)}, \tag{3.16}$$

$$\Omega = \left(\frac{\partial H}{\partial J}\right)_{Q,P,S} = \frac{\pi J(8PS+3)}{3\mathcal{M}S}. \tag{3.17}$$

Calculations show that the intensive quantities calculated by Eqs. (3.14)–(3.17) coincide with Eqs. (3.1), (3.4), (3.8) and (3.11), respectively. Thus, these thermodynamic quantities satisfy the first law of black hole thermodynamics in the enthalpy representation

$$dH = TdS + \Phi dQ + VdP + \Omega dJ. \tag{3.18}$$

In addition, for the sake of completeness, we calculate the Smarr relation. Using the scaling argument, it should be given as

$$H = 2TS + Q\Phi + 2\Omega J - 2PV. \tag{3.19}$$

A. Phase transition and stability

Thermodynamic stability tells us how a system in thermodynamic equilibrium responds to fluctuations of thermodynamic parameters. We should distinguish between global and local stability. In global stability, the preferred phase of the system is the one that minimizes the Gibbs free energy while the positivity of the heat capacity is related to local stability. Due to the presence of the nonlinearity in the structure of electrodynamic background of the solutions, we have to check both local and global stabilities as requirements of having physical solutions. These criteria are sufficiently strong to veto some models.

To investigate global stability, we use the following expression for the Gibbs free energy in terms of S, Q and J

$$G = H - TS = \frac{4J^2(128S^2P^2 + 120SP + 27) + \frac{3Q^4[3(3\Upsilon+1)+8SP(3\Upsilon-1)]}{(1+\Upsilon)\Upsilon^2}}{4S(8SP+3)\left[\frac{3}{\pi S}\left(32SJ^2P + 12J^2 + \frac{3Q^4}{\Upsilon^2}\right)\right]^{1/2}}.$$

Regarding the functional form of Gibbs free energy, it is obvious that its analytical investigation is a nontrivial task. So, we use some figures to find the behavior of G. In Fig. 6, we have shown the Gibbs free energy in terms of entropy. Considering Fig. 6(a), we find that for constant J and Q, the Gibbs free energy is a decreasing function of S for both small and large event horizon entropy, while, in general, it can be an increasing function for intermediate S. This behavior confirms that intermediate black holes are globally unstable. In addition, since the large black holes have negative Gibbs free energy, they are more stable than small black holes. Also, Fig. 6 shows that by increasing the

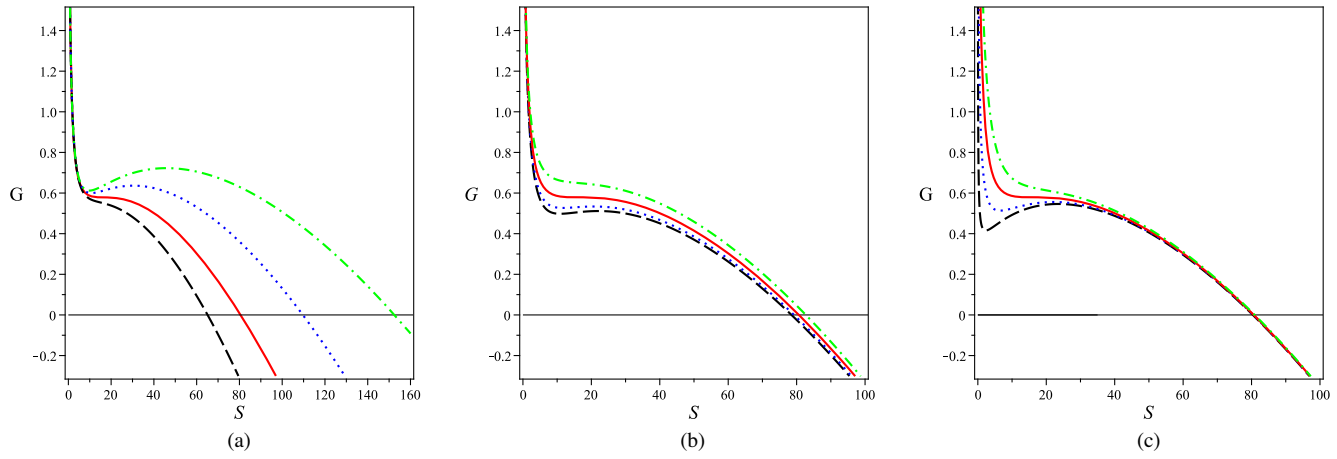

FIG. 6. The behavior of G in terms of S for $P = 0.0025 < P_{\rm crit}$, $P = 0.0035 < P_{\rm crit}$, $P = P_{\rm crit} \approx 0.0048$, $P = 0.006 > P_{\rm crit}$ and $J = 0.5$, $Q = 0.5$ (top to bottom) (left), for $P = 0.0048$, $J = 0.5$ and $Q = 0.1, 0.3, 0.5, 0.7$ (bottom to top) (middle), for $P = 0.0048$, $Q = 0.5$ and $J = 0.1, 0.3, 0.5, 0.7$ (bottom to top) (right).

pressure the black hole is more stable. Also, we have shown the behavior of the Gibbs free energy in terms of S for constant pressure and angular momentum in Fig. 6(b) and for constant pressure and electric charge in Fig. 6(c). It is obvious that by increasing the angular momentum and electric charge the black hole is more stable.

Now, we investigate the local stability by analyzing the sign of the heat capacity. The form of C_P, plotted in Fig. 7, is explicitly as follows

$$C_P = T\left(\frac{\partial S}{\partial T}\right)_P = \frac{-2S(1+\Upsilon)^2\Gamma_3(4J^2\Upsilon^2\Gamma_3 + 3Q^4)\Theta_1}{\Theta_2}, \tag{3.20}$$

where

$$\Theta_1 = \Upsilon\Gamma_3[Q^4 + 4J^2\Upsilon(1+\Upsilon)] - 3Q^4\Gamma_1$$

and

$$\begin{aligned}\Theta_2 = {} & 64J^4\Upsilon^5\Gamma_3^2\Gamma_{9/4}[\Upsilon^2 + 3(\Upsilon+1)] + 18Q^8\Gamma_{-3/2} + 4096J^4\Upsilon^4\Gamma_3\left(S^2P^2 + \frac{21}{32}SP + \frac{27}{256}\right) \\ & + 16J^2Q^4\Upsilon^2\Gamma_3^2(\Upsilon^3\Gamma_{9/2} + 3\Gamma_{3/2}) + 9Q^8\Upsilon^3\Gamma_3^2 - 3072J^2Q^4\Upsilon^4\Gamma_3\left(S^2P^2 - \frac{3}{16}SP - \frac{15}{128}\right) \\ & + 3072J^2Q^4\Upsilon^3\Gamma_3\left(S^2P^2 + \frac{15}{16}SP + \frac{21}{128}\right) - 1344Q^8\Upsilon^2\left(S^2P^2 + \frac{3}{28}SP - \frac{9}{448}\right) \\ & + 27Q^8\Upsilon\left(64S^2P^2 + \frac{20}{3}SP + 1\right),\end{aligned}$$

in which we used the abbreviation of $\Gamma_i = i + 8SP$.

Considering Fig. 7(a), one finds that there exist three different regions for $P < P_{\rm crit}$, in which the critical value of pressure, $P_{\rm crit}$ (with $T_{\rm crit}$ and $S_{\rm crit}$) can be calculated via the obtaining inflection point of isothermal P-S diagrams as follows

$$\left(\frac{\partial P}{\partial S}\right)_T = 0, \quad \text{and} \quad \left(\frac{\partial^2 P}{\partial S^2}\right)_T = 0.$$

The partially positive specific heat for both small and large black hole regions means that those black holes are thermodynamically locally stable. Having negative specific heat of the intermediate black hole region represents a locally unstable system. The unstable region disappears at pressure $P = P_{\rm crit}$ resulting in a divergence point. When $P > P_{\rm crit}$, C_P is always positive and no divergent point exists. It means that in this case the black hole is local stable for arbitrary values of S. In Figs. 7(b) and 7(c), the behavior of C_P in terms of S for different values of electric charge Q and angular momentum J of black hole has been plotted. Obviously, at the critical pressure by increasing Q and J the critical point disappears and black hole is stable.

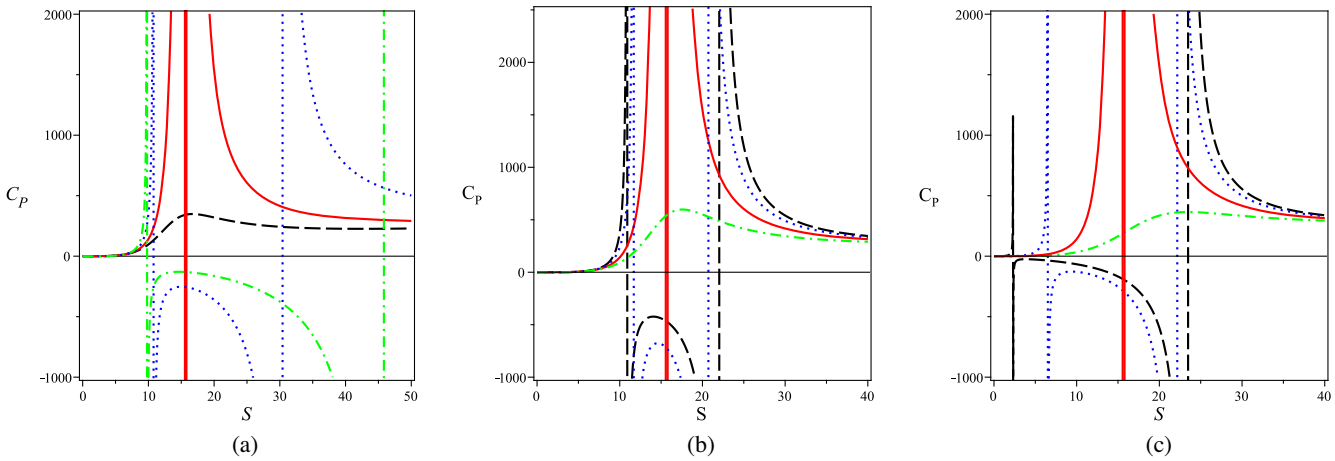

FIG. 7. The behavior of C_P in terms of S for $J = 0.5$, $Q = 0.5$, $P = 0.0025 < P_{\text{crit}}$, $P = 0.0035 < P_{\text{crit}}$, $P = P_{\text{crit}} \approx 0.0048$ and $P = 0.006 > P_{\text{crit}}$ (dotted-dashed to dashed line) (left), for $P = 0.0048$, $J = 0.5$ and $Q = 0.1$, 0.3, 0.5, 0.7 (dashed to dotted-dashed line) (middle), for $P = 0.0048$, $Q = 0.5$ and $J = 0.1$, 0.3, 0.5, 0.7 (dashed to dotted-dashed line) (right).

The behavior of heat capacity could also represent the phase transitions. It is clear that the heat capacity has at most two divergences which separate small stable black holes, unstable region with medium horizon radius, and large stable ones that are coincidence with extremum points of temperature and Gibbs free energy. Also, the root of temperature coincides with the point that the heat capacity changes its signature. The root separates the nonphysical solutions with negative temperature from physical black holes with positive temperature (Fig. 8).

At the root the temperature is zero, which corresponds to the extremal configurations of black hole and leads to the maximum of the angular momentum such that

$$J^2_{\text{max}} = \frac{(3(1-\Upsilon)+8SP(3-\Upsilon))Q^4}{4\Upsilon^2(1+\Upsilon)(3+8SP)}. \qquad (3.21)$$

The plot of the Gibbs free energy with respect to the temperature shows a swallowtail behavior as presented in Fig. 9. When $P < 0.0048$, the Gibbs free energy with respect to temperature develops a swallowtail like shape. There is a small/large first order phase transition in the black hole, which resembles the liquid/gas change of phase occurring in the van der Waals fluid. At the critical pressure $P \approx 0.0048$, the swallowtail disappears which corresponds to the critical point. In the Figs. 9(b) and 9(c), we have represented the behavior of the Gibbs free energy in terms temperature for the different values of Q and J. As can be seen, by increasing J and Q the critical point disappears.

By using Eq. (3.14), we have plotted the pressure as a function of the entropy in Fig. 10, keeping T, Q and J fixed. The temperature of isotherm diagrams decreases from top to bottom. The upper black solid line corresponds to the ideal gas phase, the critical isotherm is denoted by the red solid line, lower blue solid line corresponds to temperature smaller than the critical temperature and below the temperature the pressure becomes negative. Again, this is

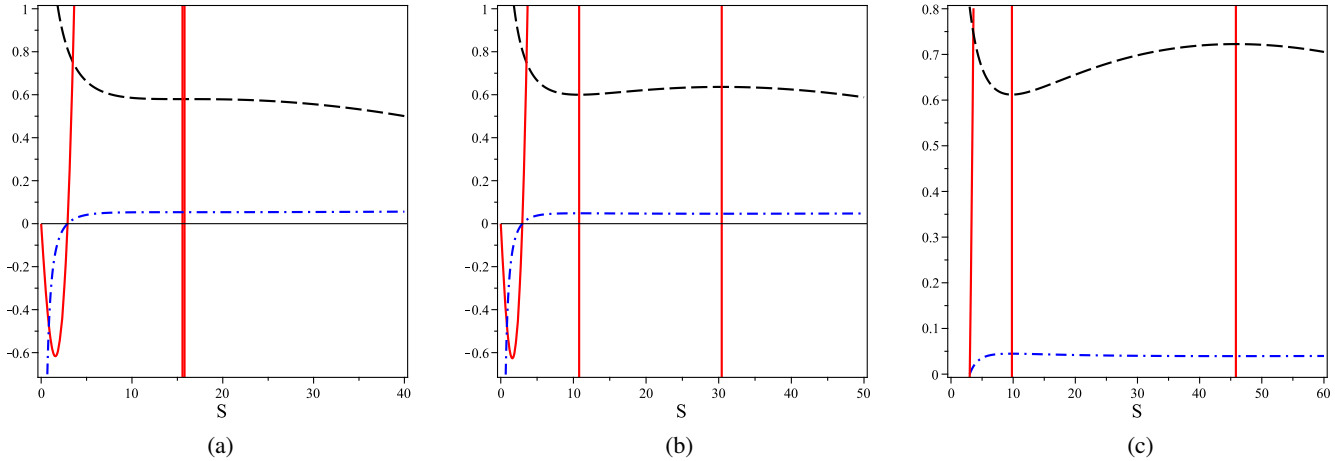

FIG. 8. The behavior of C_P (red solid line), T (blue dotted line) and G (black dashed line) in terms of S for $J = 0.5$, $Q = 0.5$, $P = 0.0048$ (left), $P = 0.0035$ (middle) and $P = 0.0025$ (right).

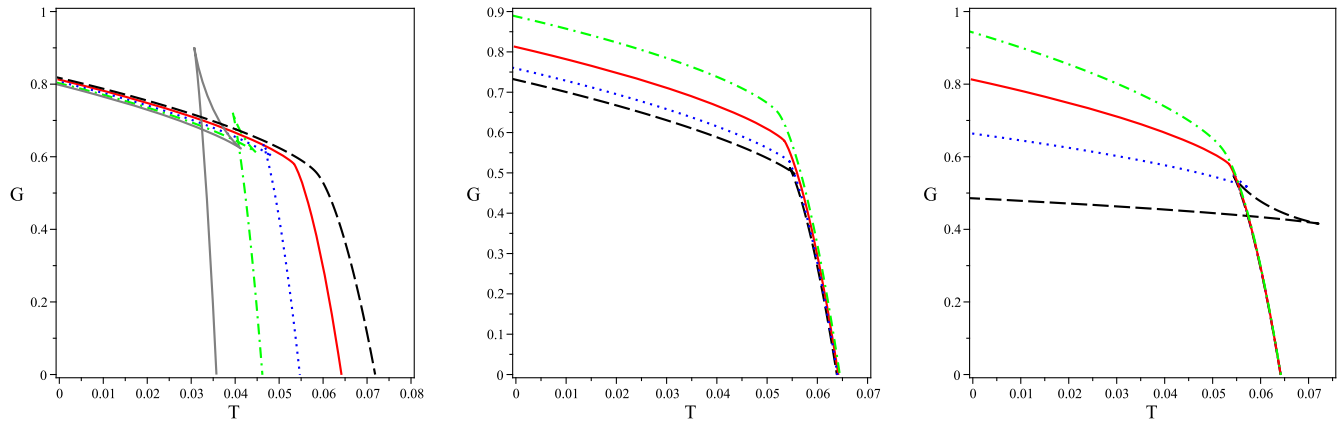

FIG. 9. The behavior of G in terms of T for $P = 0.0015 < P_{\text{crit}}$, $P = 0.0025 < P_{\text{crit}}$, $P = 0.0035 < P_{\text{crit}}$, $P = P_{\text{crit}} \approx 0.0048$, $P = 0.006 > P_{\text{crit}}$ and $J = 0.5$, $Q = 0.5$ (left to right) (left), for $P = 0.0048$, $J = 0.5$ and $Q = 0.1, 0.3, 0.5, 0.7$ (bottom to top) (middle), for $P = 0.0048$, $Q = 0.5$ and $J = 0.1, 0.3, 0.5, 0.7$ (bottom to top) (right).

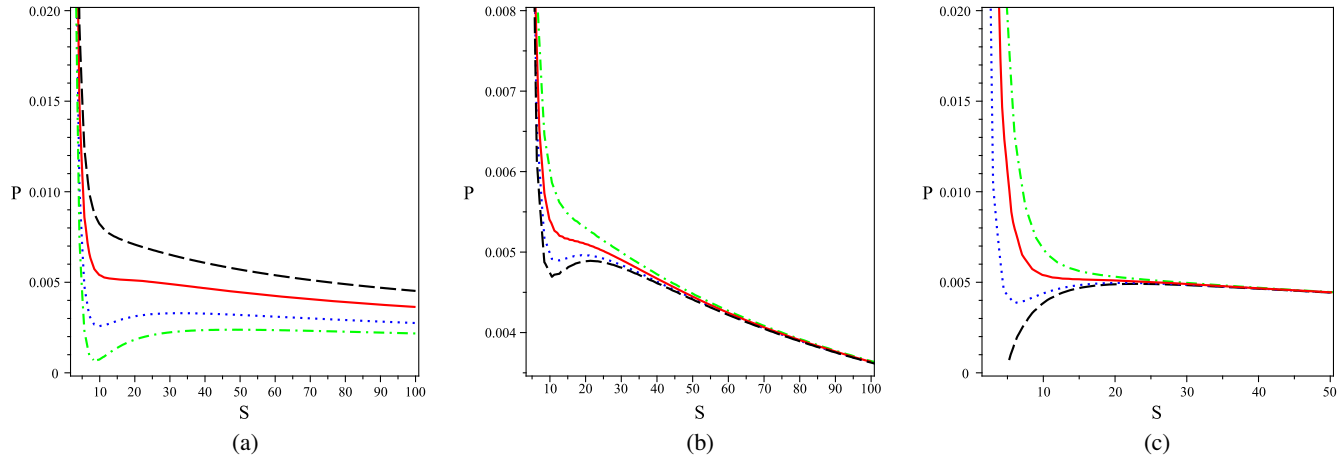

FIG. 10. The behavior of P in terms of S for $T = 0.038 < T_{\text{crit}}$, $T = 0.045 < T_{\text{crit}}$, $T = T_{\text{crit}} = 0.055$, $T = 0.065 > T_{\text{crit}}$ and $J = 0.1$, $Q = 0.1$ (top to bottom) (left), for $T = 0.055$, $J = 0.5$ and $Q = 0.1, 0.3, 0.5, 0.7$ (bottom to top) (middle), for $T = 0.055$, $Q = 0.5$ and $J = 0.1, 0.3, 0.5, 0.7$ (bottom to top) (right).

similar to the pressure-volume plot in the van der Waals liquid/gas system.

IV. QNMs

Here, we are going to calculate the QNMs of constructed black hole solutions to investigate the dynamical stability of obtained black hole solutions undergoing scalar perturbations. It is possible to obtain an analytic relation for the real and imaginary parts of QNM as functions of the black hole charges (M, a, q) and of the gravitational perturbation field (j, m). To do that, we obtain the field equation for the massless scalar probe as follows

$$\nabla_\alpha \nabla^\alpha \Phi = 0. \tag{4.1}$$

By using two Killing vectors of the metric ∂_t and ∂_ϕ, one can use the separation of variables of the scalar field as

$$\Phi(t, r, \theta, \phi) = e^{-iwt+im\phi} R(r) S(\theta). \tag{4.2}$$

Inserting Eq. (4.2) into (4.1) leads to two differential equations for the angular $S(\theta)$ and radial $R(r)$ terms of wave functions

$$\frac{d}{dr}\left(\Delta_r \frac{dR(r)}{dr}\right) + \left(\frac{\Xi^2(w^2(r^2+a^2)^2 + m^2a^2 + 2maw(\Delta_r - r^2 - a^2))}{\Delta_r} - E\right)R = 0, \tag{4.3}$$

$$\frac{d^2S(\theta)}{d\theta^2}+\cot(\theta)\frac{dS(\theta)}{d\theta}+\frac{\Xi^2}{\Delta_\theta}\left(-w^2a^2\sin^2(\theta)-\frac{m^2}{\sin^2(\theta)}+E\right)S(\theta)=0, \tag{4.4}$$

where E is a separation constant.

In order to study QNMs, first one can change the radial coordinate $r\in(r_+,\infty)$ to tortoise coordinate $x\in(-\infty,\infty)$ as follows

$$\frac{dx}{dr}=\frac{r^2+a^2}{\Delta_r},\qquad \psi(x)=\sqrt{r^2+a^2}R(r). \tag{4.5}$$

Now, we can find that black hole perturbations from Eq. (4.3) can be reduced to the following second-order ordinary differential equation

$$\frac{d^2\psi(x)}{dx^2}+Q(x,w)\psi(x)=0, \tag{4.6}$$

where

$$Q(x,w)=w^2+\frac{a^2m^2-4amwf(r)-E\Delta_r(r)}{(r^2+a^2)^2}-\frac{r\Delta_r\Delta_r'}{(r^2+a^2)^3}+\frac{\Delta_r^2(2r^2-a^2)}{(r^2+a^2)^4}. \tag{4.7}$$

So, for the slowly rotating and small charged black hole $a\ll 1$, $\Lambda=0$ and for the case $j\gg 1$ and $m\gg 1$, the effective potential becomes

$$Q=w^2-V\approx w^2-\left(1-\frac{2M}{r}e^{-\frac{q^2}{2Mr}}\right)\frac{j(j+1)}{r^2}-\frac{4mMwa}{r^3}e^{-\frac{q^2}{2Mr}}. \tag{4.8}$$

By using of Mashhoon's method [69,70] for QNMs, we can obtain an approximate expression for quasinormal frequencies. The parameter set here is $p=(M,q,am,w,\lambda)$, which is transformed into $p'=(-iM,-iq,-am,\Omega,-\lambda)$ and $x\to -ix$ so that

$$W(x;\Omega)\approx\left(1-\frac{2M}{r}e^{-\frac{q^2}{2Mr}}\right)\frac{j(j+1)\lambda}{r^2}-\frac{4amM\Omega\lambda}{r^3}e^{-\frac{q^2}{2Mr}} \tag{4.9}$$

and the quasinormal mode problem is converted to finding the bound states $\Omega>0$ of $-W(x;\Omega)$. So, by using the analytic approximation formulas (B6)–(B8), the maximum of W occurs at

$$r_{ps}=3M\left(1+\frac{2ma\Omega}{j(j+1)}\right)-\frac{2q^2}{3M}-\frac{17q^4}{216M^3}\left(1-\frac{2ma\Omega}{j(j+1)}\right), \tag{4.10}$$

and therefore, r_{ps} is the radius of the photon sphere. The value of the maximum potential is

$$W_m=\frac{j(j+1)\lambda}{27M^2}\left(1+\frac{q^2}{3M^2}+\frac{13q^4}{81M^4}\right)-\frac{4ma\Omega\lambda}{27M^2}\left(1+\frac{q^2}{2M^2}+\frac{13q^4}{54M^4}\right) \tag{4.11}$$

and the curvature parameter is given by [69,70]

$$\alpha=\frac{\sqrt{3}}{9M}\left(1+\frac{5q^2}{18M^2}+\frac{23q^4}{216M^4}\right)-\frac{2\sqrt{3}ma\Omega}{3Mj(j+1)}\left(1+\frac{26q^2}{54M^2}+\frac{41q^4}{162M^4}\right).$$

It should be noted that Ω has a crucial role for all the above results. In order to obtain Ω, we have inserted the above results in Eq. (B8). Solving second-order equation for Ω, one can find the proper quasinormal frequencies as follows

$$w_r+iw_i=\Omega(iM,iq,-am,-1), \tag{4.12}$$

where λ is scaling parameter. The real and imaginary parts of frequency are, respectively,

$$w_r=\frac{(j+\frac{1}{2})}{3\sqrt{3}M}\left(1+\frac{q^2}{6M^2}+\frac{43q^4}{648M^4}\right)+\frac{2ma}{27M^2}\left(1+\frac{q^2}{2M^2}+\frac{13q^4}{54M^4}\right), \tag{4.13}$$

and

$$w_i=\frac{(n+\frac{1}{2})}{3\sqrt{3}M}\left(1+\frac{5q^2}{18M^2}+\frac{23q^4}{216M^4}\right)+\frac{8ma(n+\frac{1}{2})}{27M^2j}\left(1+\frac{23q^2}{36M^2}+\frac{983q^4}{2592M^4}\right), \tag{4.14}$$

where $n = 0, 1, 2, \ldots$ ($n \ll j$). The rotation remove the $(2j+1)$-fold degeneracy of the spherical modes both in real and imaginary part of frequencies in contrast to the Schwarzschild black hole where the imaginary part of frequencies still remains degenerate. Moreover, in the eikonal approximation under consideration Eqs. (4.13) and (4.14) are independent of the spin of the perturbing field and agree with the results obtained previously in [69,70].

As a final point, we should note that there is a relation between the quasinormal frequencies and the properties of photon orbits in the eikonal limit. It is noted that the real part of the quasinormal frequencies is related to the angular velocity of the photon orbit while the imaginary part may be related to the Lyapunov exponent. A careful attention can be helped to confirm the fact that there is a good agreement between the Lyapunov exponent and imaginary part of quasinormal frequency. We examine these statements in the following subsection.

A. Connection between QNMs and photon sphere in the eikonal limit

In what follows, we want to investigate the relation between the real part of quasinormal modes and the radius of the shadow cast by the photon sphere of the black hole. To do so, we use the Hamilton-Jacobi Method to obtain the following equations of motion for null geodesics of charged rotating regular black hole at equatorial plane (see Appendix A) [36,89]

$$\Sigma\left(\frac{dr}{d\gamma}\right) = \sqrt{R(r)}, \qquad \Theta(\theta) = \sqrt{k},$$
$$\Sigma\left(\frac{dt}{d\gamma}\right) = T, \qquad \Sigma\left(\frac{d\phi}{d\gamma}\right) = \varphi, \tag{4.15}$$

where

$$R(r) = E^2(r^2 + a^2 - a\xi)^2 \times \left(1 - \frac{[r^2 + a^2 - 2f(r)][\eta + (\xi - a)^2]}{(r^2 + a^2 - a\xi)^2}\right), \tag{4.16}$$

$$T = E^2\left[\frac{r^2 + a^2}{\Delta}(r^2 + a^2 - a\xi) - a(a - \xi)\right], \tag{4.17}$$

$$\varphi = E^2\left[\frac{a}{\Delta}(r^2 + a^2 - a\xi) - (a - \xi)\right], \tag{4.18}$$

and

$$\xi = \frac{L}{E}, \qquad \eta = \frac{k}{E^2} \tag{4.19}$$

are two impact parameters. The conditions for the unstable circular orbits is given by $R(r) = dR(r)/dr = 0$. Now, one can easily obtain the expressions for ξ and η from the conditions of unstable circular orbits. For the generic $f(r)$, these parameters take the following simple forms

$$\xi = \frac{(a^2 + r^2)[r + f'(r)] - 4rf(r)}{a[f'(r) - r]}, \tag{4.20}$$

$$\eta = \frac{r^2[8f(r^2 + a^2) + 8rff' - 16f^2 - 2r^3f' - r^2f'^2 - 4ra^2f' - r^4]}{a^2(r - f')^2}, \tag{4.21}$$

where r is the radius of the unstable circular orbits. These two equations determine the contour of the shadow in $\xi - \eta$ plane. Furthermore, the radius of the shadow is calculated as

$$R_s^2 = \xi^2 + \eta = \frac{\left(1 + \frac{(a^2+2r^2)q^2}{2(a^2-6r^2)Mr}\right)(a^2 - 6r^2)M^2 + a^2(q^2 + 2Mr)e^{\frac{q^2}{2Mr}} + r^2(a^2 + 2r^2)e^{\frac{q^2}{Mr}}}{\left(M - re^{\frac{q^2}{2Mr}}\right)^2}$$

in which for the limit of $q \ll 1$, $a \ll 1$ and $j \gg 1$, we have

$$R_s^2 \approx \frac{2r^2(r^2 - 3M^2)}{(r - M)^2} + \frac{4Mrq^2}{(r - M)^2} + \frac{(r^2 + Mr - 4M^2)q^4}{2M(r - M)^3}. \tag{4.22}$$

By inserting $w = \sqrt{w_r^2 + w_i^2}$ into the Eq. (4.10), one can obtain the radius of photon sphere as follows

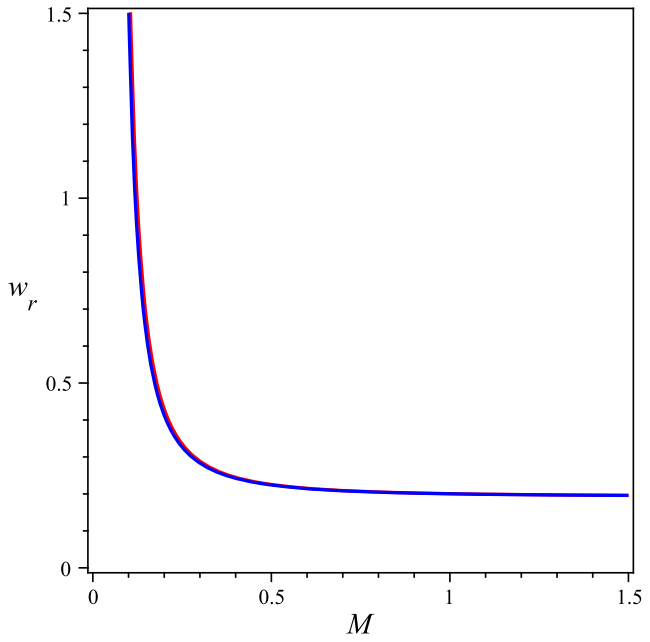

FIG. 11. The comparison between w_r in Eq. (4.24) (red solid line) and Eq. (4.13) (blue solid line).

$$r = r_{ps} \approx 3M\left(1 - \frac{2q^2}{9M^2} - \frac{17q^4}{648M^4}\right) - \frac{2ma}{3\sqrt{3}jM}\left(1 + \frac{q^2}{6M^2} + \frac{17q^4}{648M^4}\right). \quad (4.23)$$

It is obvious that in the limit $q \ll 1$, $a \ll 1$ and by inserting Eq. (4.23) for r_{ps} (at $j = m$) into the Eq. (4.22), we achieve

$$R_s = 3\sqrt{3}M - 4a - \frac{\sqrt{3}q^2}{2M} - \frac{q^4}{24\sqrt{3}M^3} + \frac{4aq^4}{3M^4},$$

and it is easy to show that the real part of QNMs is inversely proportional to the shadow radius as follows

$$w_r \approx \frac{j}{R_s} = \frac{j}{3\sqrt{3}M}\left(1 + \frac{q^2}{3M^2} + \frac{13q^4}{108M^4}\right) + \frac{4ma}{27M^2}\left(1 + \frac{2q^2}{3M^2} + \frac{35q^4}{108M^4}\right), \quad \text{for } j \gg 1. \quad (4.24)$$

In Fig. 11, we have done a comparison between real part of quasi normal modes in Eq. (4.24) and Eq. (4.13). As, can be seen, there is a good agreement between them.

In the following, we want to obtain the connection between Lyapunov exponent and the imaginary parts of quasinormal mode [Eq. (4.14)]. The Lyapunov behavior exists in the systems that sensitive to the initial conditions. So, the Lyapunov exponent which determines the value of the sensitivity should have behavior looks like the imaginary parts of quasinormal mode which determines instability of black hole. To extract the Lyapunov exponent, we follow the method of Ref. [70]. We perturb the equatorial geodesic equations (4.15) as

$$r = r_{ps}[1 + \epsilon f(t)],$$
$$\gamma = t + \epsilon h(t),$$
$$\phi = |w_+|[t + \epsilon g(t)].$$

Here, by perturbing the radial equation to leading order in ϵ, we obtain

$$2\dot{t}^2\frac{d^2f(t)}{dt^2} + \frac{d^2V}{dr^2}f(t)\Big|_{r_{ps}} = 0. \quad (4.25)$$

Now, by solving Eq. (4.25) and using the condition $f(0) = 0$, we can find

$$f(t) = \sinh(\varsigma t), \qquad \varsigma = \sqrt{-\frac{1}{2\dot{t}^2}\frac{d^2V}{dr^2}\Big|_{r_{ps}}}.$$

So, by using of first equation for the radial and third equation for t of Eqs. (4.15) and (4.20) and also the Eq. (4.10) for photon sphere radius in the limit of $q \ll 1$, $a \ll 1$ and $j \gg 1$, we can write

$$\varsigma = \frac{j}{3\sqrt{3}M}\left(1 + \frac{4q^2}{9M^2} + \frac{49q^4}{324M^4}\right) + \frac{8ma}{27jM^2}\left(1 + \frac{2q^2}{3M^2} + \frac{20q^4}{81M^4}\right).$$

For the sake of completeness, we have done a comparison between Lyapunov exponent and imaginary part of quasinormal frequency in Fig. 12, and obviously, there is a good agreement between them.

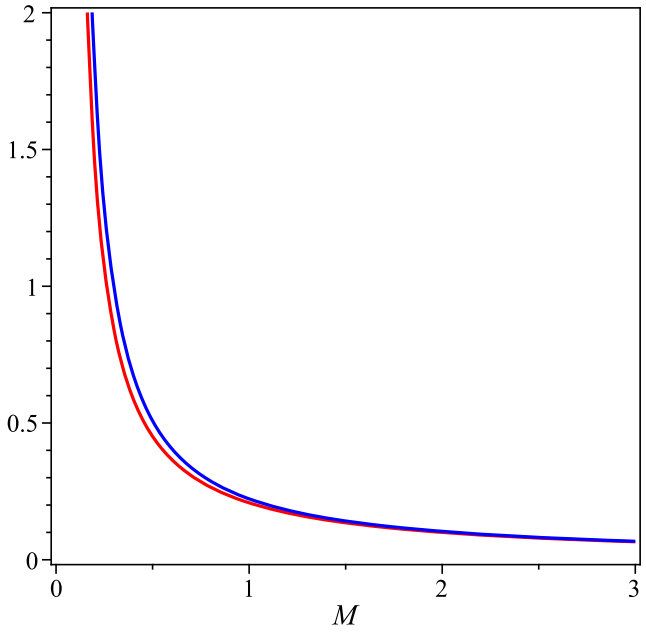

FIG. 12. The comparison of ς (red line) and w_i (blue line) in terms of M for $a = q = 0.1$.

V. CONCLUSION

In this study, we have addressed a rotating regular black hole in the framework of Einstein's general relativity coupled to a nonlinear electrodynamics. We have shown that for some values of parameters, there is an event horizon for nonsingular solution and we can interpret it as a black hole. In fact, we have obtained an upper limit for the magnetic charge or rotation parameter in order to have event horizon and ergosphere. We have plotted the ergoregion and have shown that, as the magnetic charge and rotation parameter increased, the ergoregion also increased. Since thermodynamical behavior is of great importance in the search for a quantum theory of gravitation, we have also managed to perform a thermodynamic investigation of the black hole solutions. The conserved and thermodynamic quantities have been calculated and the validity of the first law has been examined. In addition, we have investigated the global stability of the black hole by plotting the Gibbs free energy. Also, the heat capacity has been studied to check the local stability. We have shown that the present solutions admitted small/large phase transitions similar to the van der Waals liquid/gas phase transition. Then, we have analytically studied the quasinormal modes of black hole by using of Mashhoon's method. Finally, in order to obtain a relation between the quasinormal frequencies and the properties of the photon sphere, we have obtained the shadow radius of black hole and Lyapunov exponent. As it can be seen, there is a good agreement between the inverse of shadow radius and Lyapunov exponent with real and imaginary parts of quasinormal modes, respectively.

It is interesting to obtain a relation between thermodynamical quantities and quasinormal frequencies like [77,78,90] in which a relation between the first law of thermodynamics and real part of quasinormal frequencies in some conditions has been obtained. We leave these work for future work.

ACKNOWLEDGMENTS

The authors would like to thank the referees for their fruitful comments. S. H. H. and S. N. S. thank Shiraz University Research Council. M. K. thanks the support of Shahid Beheshti University.

APPENDIX A: EFFECTIVE POTENTIAL

Here, we want to show why we have used the original metric instead of effective metric to study the shadow of black hole. As we know, photons in the nonlinear electrodynamics do follow the null geodesics of an effective metric rather than of the original one [36]. So, we need to study the effective metric. The effective geometry has been written as follows

$$g_{\rm eff}^{\mu\nu} = L_F g^{\mu\nu} - 4L_{FF}F^{\mu}_{\alpha}F^{\alpha\nu}. \tag{A1}$$

So the effective metric in the plane $\theta = \pi/2$ can be written as

$$ds^2 = g_{tt}^{\rm eff}dt^2 + g_{rr}^{\rm eff}dr^2 + 2g_{t\phi}^{\rm eff}dtd\phi + g_{\phi\phi}^{\rm eff}d\phi^2, \tag{A2}$$

where

$$g_{tt}^{\rm eff} = \frac{-L_F r^6 + 2L_F f r^4 + 4L_{FF}a^2q^2 + 4L_{FF}q^2r^2 - 8L_{FF}fq^2}{L_F r^2(L_F r^4 - 4L_{FF}q^2)}, \tag{A3}$$

$$g_{rr}^{\rm eff} = \frac{r^2}{L_F(a^2 + r^2 - 2f)}, \tag{A4}$$

$$g_{t\phi}^{\rm eff} = -\frac{2a(-L_F f r^4 - 2L_{FF}a^2q^2 - 2L_{FF}q^2r^2 + 4L_{FF}fq^2)}{r^2L_F(-L_F r^4 + 4L_{FF}q^2)}, \tag{A5}$$

$$g_{\phi\phi}^{\rm eff} = \frac{-L_F a^2 r^6 - L_F r^8 - 2L_F a^2 f r^4 - 4L_{FF}a^4q^2 - 4L_{FF}a^2q^2r^2 + 8L_{FF}a^2fq^2}{r^2L_F(-L_F r^4 + 4L_{FF}q^2)}. \tag{A6}$$

Here L_F is the same as that of Eq. (2.15) but at $\theta = \pi/2$ and $L_{FF} = dL_F/dF$ at $\theta = \pi/2$. It is useful to study the effective potential that is felt by the photons. By using of the symmetries of the metric one can achieve to the following equation

$$\frac{1}{2}\dot{r}^2 + V_{\rm eff} = \Xi, \tag{A7}$$

where

$$V_{\rm eff} = \frac{1}{2g_{rr}}(g_{tt}\dot{t}^2 + 2g_{t\phi}\dot{t}\dot{\phi} + g_{\phi\phi}\dot{\phi}^2),$$
$$E = g_{\alpha\beta}\xi_t^{\alpha}\dot{x}^{\beta},$$
$$L = g_{\alpha\beta}\xi_{\phi}^{\alpha}\dot{x}^{\beta},$$

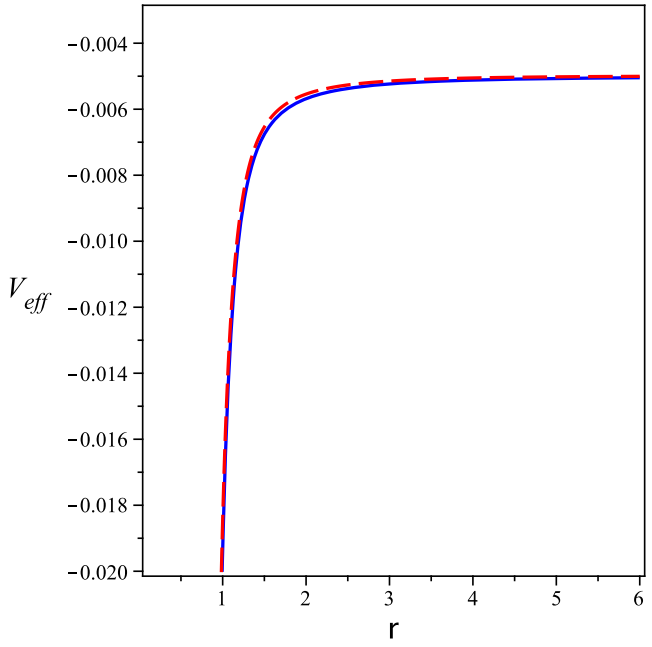

FIG. 13. The behavior of effective potential in terms of r for $M = 1$, $\theta = \frac{\pi}{2}$, $b = \frac{E}{L} = 0.1$, $q = 0.5$, $a = 0.5$ (dashed line for metric (2.4) and solid line for metric (A2).

and g_{ab} are the components of the metric, ξ is the Killing vector and Ξ is the total energy. Considering Fig. 13, we give plots of V_{eff} for the metric (A2)(blue line) and for metric (2.4)(red line). One can see that the difference between the two plots is insignificant and it is thus legitimate to use the original metric instead of effective one.

APPENDIX B: A BRIEF REVIEW ON MASHHOON'S METHOD

According to this method the QNMs of a potential barrier are related to the bound states of the inverted potential [69,70]. Let p be a set of parameters associated with the potential. These may belong to the potential already, or they may be simply introduced as scaling parameters. The parametrized potential is denoted by $U(x; p)$; the wave functions and the quasinormal frequencies arc also functions of the parameters p:$\psi = \psi(x; p)$ and $w = w(p)$. Consider the formal transformations $x \to -ix$ and $p \to p' = \Pi(p)$ in such a way that the potential remains invariant

$$U(-ix; p') = U(x; p). \tag{B1}$$

Let us define ϕ and Ω such that

$$\phi(x; p) = \psi(-ix; p') \quad \text{and} \quad \Omega(p) = w(p'). \tag{B2}$$

Then ϕ satisfies the Schrödinger equation

$$\frac{d^2\phi}{dx^2} + (-\Omega^2 + U)\phi = 0 \tag{B3}$$

and the boundary conditions for the QNMs are reduced to

$$\phi(x; p) \propto \exp(\mp\Omega x) \quad \text{as } x \to \pm\infty. \tag{B4}$$

Once $\Omega(p)$ is determined, the QNMs are found by the inverse transformation

$$w(p) = \Omega(\Pi^{-1}(p)) \quad \text{and} \quad \psi(x; p) = \phi(ix; \Pi^{-1}(p)). \tag{B5}$$

The QNMs which are directly related, through Eq. (B5), to the true bound states of the inverted potential will be referred to proper QNMs. For instance, consider $U(x)$ drops exponentially to zero for $x \to -\infty$, but falls off as x^{-2} for $x \to +\infty$. In this case, one can estimate $U(x)$ by using simpler potentials that approximate it closely near its maximum. This simple potential is the Poschl-Teller potential

$$U_{PT} = \frac{U_0}{\cosh^2 \alpha(x - x_0)}. \tag{B6}$$

The quantities U_0 and $\alpha > 0$ are given by the height and curvature of the potential at its maximum ($x = x_0$). Thus,

$$U_0 = U(x_0), \qquad \alpha^2 = -\frac{1}{2U_0}\frac{d^2U}{dx^2}\bigg|_{x_0}. \tag{B7}$$

The transition from the potential barrier U_{PT} to the inverted potential is achieved by the transformations $x \to -ix$, $(U_0, \alpha) \to (U_0, i\alpha)$. The bound states of $-U_{PT}$ are given by

$$\Omega_n(U_0, \alpha) = \alpha\left[-\left(n + \frac{1}{2}\right) + \left(\frac{1}{4} + \frac{U_0}{\alpha^2}\right)^{\frac{1}{2}}\right]. \tag{B8}$$

The proper QNMs may be obtained from $\Omega_n(U_0, -i\alpha)$ corresponding frequencies are given by

$$w_r = \pm\left(U_0 - \frac{\alpha^2}{4}\right)^{\frac{1}{2}}, \qquad w_i = \alpha\left(n + \frac{1}{2}\right). \tag{B9}$$

[1] J. Bardeen, in *Conference Proceedings of GR5* (USSR, Tbilisi, 1968), p. 174.
[2] E. Ayon-Beato and A. Garcia, Phys. Rev. Lett. **80**, 5056 (1998).
[3] E. Ayon-Beato and A. Garcia, Phys. Lett. B **464**, 25 (1999).
[4] E. Ayon-Beato and A. Garcia, Gen. Relativ. Gravit. **31**, 629 (1999).
[5] E. Ayon-Beato and A. Garcia, Phys. Lett. B **493**, 149 (2000).
[6] L. Balart and E. C. Vagenas, Phys. Rev. D **90**, 124045 (2014).
[7] S. G. Ghosh, Eur. Phys. J. C **75**, 532 (2015).
[8] S. N. Sajadi and N. Riazi, Gen. Relativ. Gravit. **49**, 45 (2017).
[9] K. A. Bronnikov, Phys. Rev. D **64**, 064013 (2001).
[10] K. A. Bronnikov, Particles **1**, 56 (2018).
[11] K. A. Bronnikov, Phys. Rev. D **96**, 128501 (2017).
[12] K. Bronnikov, Phys. Rev. Lett. **85**, 4641 (2000).
[13] K. Bronnikov and J. Fabris, Phys. Rev. Lett. **96**, 251101 (2006).
[14] S. A. Hayward, Phys. Rev. Lett. **96**, 031103 (2006).
[15] W. Berej, J. Matyjasek, D. Tryniecki, and M. Woronowicz, Gen. Relativ. Gravit. **38**, 885 (2006).
[16] I. Dymnikova and E. Galaktionov, Classical Quant. Grav. **22**, 2331 (2005).
[17] H. Culetu, Int. J. Theor. Phys. **54**, 2855 (2015).
[18] I. Dymnikova, Int. J. Mod. Phys. D **12**, 1015 (2003).
[19] B. Toshmatov, B. Ahmedov, A. Abdujabbarov, and Z. Stuchlik, Phys. Rev. D **89**, 104017 (2014).
[20] B. Toshmatov, Z. Stuchlík, and B. Ahmedov, Phys. Rev. D **95**, 084037 (2017).
[21] I. Dymnikova, Gen. Relativ. Gravit. **24**, 235 (1992).
[22] B. P. Abbott *et al.* (LIGO Scientific and Virgo Collaborations), Phys. Rev. Lett. **116**, 061102 (2016).
[23] B. P. Abbott *et al.* (LIGO Scientific and Virgo Collaborations), Phys. Rev. Lett. **116**, 241103 (2016).
[24] B. P. Abbott *et al.* (LIGO Scientific and Virgo Collaborations), Phys. Rev. Lett. **118**, 241103 (2017).
[25] K. Akiyama *et al.* (Event Horizon Telescope), Astrophys. J. **875**, L1 (2019).
[26] K. Akiyama *et al.* (Event Horizon Telescope), Astrophys. J. Lett. **875**, L5 (2019).
[27] K. Akiyama *et al.* (Event Horizon Telescope), Astrophys. J. Lett. **875**, L6 (2019).
[28] K. Akiyama *et al.* (Event Horizon Telescope), Astrophys. J. Lett. **875**, L4 (2019).
[29] E. T. Newman and A. I. Janis, J. Math. Phys. (N.Y.) **6**, 915 (1965).
[30] I. Dymnikova and E. Galaktionov, Classical Quant. Grav. **32**, 165015 (2015).
[31] S. P. Drake and P. Szekeres, Gen. Relativ. Gravit. **32**, 445 (2000).
[32] C. Bambi and L. Modesto, Phys. Lett. B **721**, 329 (2013).
[33] S. P. Drake and R. Turolla, Classical Quant. Grav. **14**, 1883 (1997).
[34] D. J. C. Lombardo, Classical Quant. Grav. **21**, 1407 (2004).
[35] R. Ferraro, Gen. Relativ. Gravit. **46**, 1705 (2014).
[36] M. Novello, V. A. De Lorenci, J. M. Salim, and R. Klippert, Phys. Rev. D **61**, 045001 (2000).
[37] L. Modesto and P. Nicolini, Phys. Rev. D **82**, 104035 (2010).
[38] Y. Liao, X. B. Gong, and J. S. Wu, Astrophys. J. **835**, 247 (2017).
[39] K. Jafarzade and J. Sadeghi, arXiv:1710.08642.
[40] R. T. Ndongmo, S. Mahamat, T. B. Bouetou, and T. C. Kofane, arXiv:1911.12521.
[41] S. Haroon, M. Jamil, K. Jusufi, K. Lin, and R. B. Mann, Phys. Rev. D **99**, 044015 (2019).
[42] M. Rizwan, M. Jamil, and K. Jusufi, Phys. Rev. D **99**, 024050 (2019).
[43] D. Kastor, S. Ray, and J. Traschen, Classical Quant. Grav. **27**, 235014 (2010).
[44] F. Simovic and R. B. Mann, J. High Energy Phys. 05 (2019) 136.
[45] F. Simovic and R. B. Mann, Classical Quant. Grav. **36**, 014002 (2019).
[46] L. Balart and S. Fernando, Mod. Phys. Lett. A **32**, 1750219 (2017).
[47] L. Balart and E. C. Vagenas, Phys. Lett. B **730**, 14 (2014).
[48] L. Gulin and I. Smolic, Classical Quant. Grav. **35**, 025015 (2018).
[49] D. A. Rasheed, arXiv:hep-th/9702087.
[50] N. Breton, Gen. Relativ. Gravit. **37**, 643 (2005).
[51] B. P. Dolan, Classical Quant. Grav. **28**, 125020 (2011).
[52] B. P. Dolan, Classical Quant. Grav. **28**, 235017 (2011).
[53] M. Cvetic, G. W. Gibbons, D. Kubiznak, and C. N. Pope, Phys. Rev. D **84**, 024037 (2011).
[54] D. Kubiznak and R. B. Mann, J. High Energy Phys. 07 (2012) 033.
[55] S. Gunasekaran, R. B. Mann, and D. Kubiznak, J. High Energy Phys. 11 (2012) 110.
[56] A. Belhaj, M. Chabab, H. El Moumni, and M. B. Sedra, Chin. Phys. Lett. **29**, 100401 (2012).
[57] R. Banerjee and D. Roychowdhury, Phys. Rev. D **85**, 104043 (2012).
[58] S. H. Hendi and M. H. Vahidinia, Phys. Rev. D **88**, 084045 (2013).
[59] N. Altamirano, D. Kubiznak, R. B. Mann, and Z. Sherkatghanad, Classical Quant. Grav. **31**, 042001 (2014).
[60] N. Altamirano, D. Kubiznak, R. B. Mann, and Z. Sherkatghanad, Galaxies **2**, 89 (2014).
[61] D. Kubiznak and R. B. Mann, Can. J. Phys. **93**, 999 (2015).
[62] H. Nollert, Phys. Rev. D **47**, 5253 (1993).
[63] S. Hod, Phys. Rev. Lett. **81**, 4293 (1998).
[64] G. T. Horowitz and V. E. Hubeny, Phys. Rev. D **62**, 024027 (2000).
[65] V. Cardoso and J. P. S. Lemos, Phys. Rev. D **64**, 084017 (2001).
[66] K. D. Kokkotas and B. G. Schmidt, Living Rev. Relativity **2**, 2 (1999).
[67] E. Berti, V. Cardoso, and A. O. Starinets, Classical Quant. Grav. **26**, 163001 (2009).
[68] R. A. Konoplya and A. Zhidenko, Rev. Mod. Phys. **83**, 793 (2011).
[69] V. Ferrari and B. Mashhoon, Phys. Rev. D **30**, 295 (1984).
[70] B. Mashhoon, Phys. Rev. D **31**, 290 (1985).
[71] Y. Dcanini, A. Folacci, and B. Raffaelli, Phys. Rev. D **81**, 104039 (2010).
[72] S. Fernando and J. Correa, Phys. Rev. D **86**, 064039 (2012).

[73] A. Flachi and J. Lemos, Phys. Rev. D **87**, 024034 (2013).
[74] S. C. Ulhoa, Braz. J. Phys. **44**, 380 (2014).
[75] R. A. Konoplya and A. Zhidenko, J. High Energy Phys. 09 (2017) 139.
[76] S. N. Sajadi, N. Riazi, and S. H. Hendi, Eur. Phys. J. C **79**, 775 (2019).
[77] S. Hod, Phys. Rev. Lett. **81**, 4293 (1998).
[78] S. Musiri and G. Siopsis, Phys. Lett. B **579**, 25 (2004).
[79] V. Cardoso, A. S. Miranda, E. Berti, H. Witek, and V. T. Zanchin, Phys. Rev. D **79**, 064016 (2009).
[80] I. Z. Stefanov, S. S. Yazadjiev, and G. G. Gyulchev, Phys. Rev. Lett. **104**, 251103 (2010).
[81] K. Jusufi, Phys. Rev. D **101**, 084055 (2020).
[82] K. Jusufi, Phys. Rev. D **101**, 124063 (2020).
[83] M. R. Brown, in *Proceedings, Quantum Gravity* (Oxford, 1980), pp. 439–448, https://inspirehep.net/literature/161994.
[84] J. W. Moffat, arXiv:hep-ph/0102088.
[85] R. M. Corless, G. H. Gonnet, D. E. G. Hare, D. J. Jeffrey, and D. E. Knuth, Adv. Comput. Math. **5**, 329 (1996).
[86] Z. Y. Fan and X. Wang, Phys. Rev. D **94**, 124027 (2016).
[87] E. Altas and B. Tekin, Phys. Rev. D **99**, 044026 (2019).
[88] M. M. Caldarelli, G. Cognola, and D. Klemm, Classical Quant. Grav. **17**, 399 (2000).
[89] R. Takahashi, Publ. Astron. Soc. Jpn. **57**, 273 (2005).
[90] E. Berti, V. Cardoso, K. D. Kokkotas, and H. Onozawa, Phys. Rev. D **68**, 124018 (2003).